

Article

Supramolecular Optimization of Sensory Function of a Hemicurcuminoid through Its Incorporation into Phospholipid and Polymeric Polydiacetylenic Vesicles: Experimental and Computational Insight

Bulat S. Akhmadeev ^{1,*}, Olga O. Retyunskaya ², Sergey N. Podyachev ¹, Sergey A. Katsyuba ¹, Aidar T. Gubaidullin ¹, Svetlana N. Sudakova ¹, Victor V. Syakaev ¹, Vasily M. Babaev ¹, Oleg G. Sinyashin ¹ and Asiya R. Mustafina ¹

¹ Arbuzov Institute of Organic and Physical Chemistry, FRC Kazan Scientific Center of RAS, 8 Arbuzov St., 420088 Kazan, Russia

² Department of Organic and Medicinal Chemistry, Kazan (Volga region) Federal University, Kremlyovskaya Str., 18, 420008 Kazan, Russia

* Correspondence: bulat_ahmadeev@mail.ru

Abstract: This work presents the synthesis of a new representative of hemicurcuminoids with a non-oxo substituent (**HCur**) as a fluorescent amphiphilic structural element of vesicular aggregates based on phosphatidylcholine (PC), phosphatidylserine (PS), and 10,12-pentacosadiynoic acid (PCDA). Both X-ray diffraction analysis of the single crystal and ¹H NMR spectra of **HCur** in organic solvents indicate the predominance of the enol-tautomer of **HCur**. DFT calculations show the predominance of the enol tautomer **HCur** in supramolecular assemblies with PC, PS, and PCDA molecules. The results of the molecular modeling show that **HCur** molecules are surrounded by PC and PS with a rather weak exposure to water molecules, while an exposure of **HCur** molecules to water is enhanced under its supramolecular assembly with PCDA molecules. This is in good agreement with the higher loading of **HCur** into PC(PS) vesicles compared to PCDA vesicles converted into polydiacetylene (PDA) ones by photopolymerization. **HCur** molecules incorporated into **HCur**-PDA vesicles exhibit greater planarity distortion and hydration effect in comparison with **HCur**-PC(PS) ones. **HCur**-PDA is presented as a dual fluorescence-chromatic nanosensor responsive to a change in pH within 7.5–9.5, heavy metal ions and polylysine, and the concentration-dependent fluorescent response is more sensitive than the chromatic one. Thus, the fluorescent response of **HCur**-PDA allows for the distinguishing between Cd²⁺ and Pb²⁺ ions in the concentration range 0–0.01 mM, while the chromatic response allows for the selective sensing of Pb²⁺ over Cd²⁺ ions at their concentrations above 0.03 mM.

Keywords: polydiacetylene; hemicurcuminoids; sensor



Citation: Akhmadeev, B.S.; Retyunskaya, O.O.; Podyachev, S.N.; Katsyuba, S.A.; Gubaidullin, A.T.; Sudakova, S.N.; Syakaev, V.V.; Babaev, V.M.; Sinyashin, O.G.; Mustafina, A.R. Supramolecular Optimization of Sensory Function of a Hemicurcuminoid through Its Incorporation into Phospholipid and Polymeric Polydiacetylenic Vesicles: Experimental and Computational Insight. *Polymers* **2023**, *15*, 714. <https://doi.org/10.3390/polym15030714>

Academic Editors: Yun Lu, He Liu and Jingpeng Li

Received: 11 December 2022

Revised: 18 January 2023

Accepted: 28 January 2023

Published: 31 January 2023



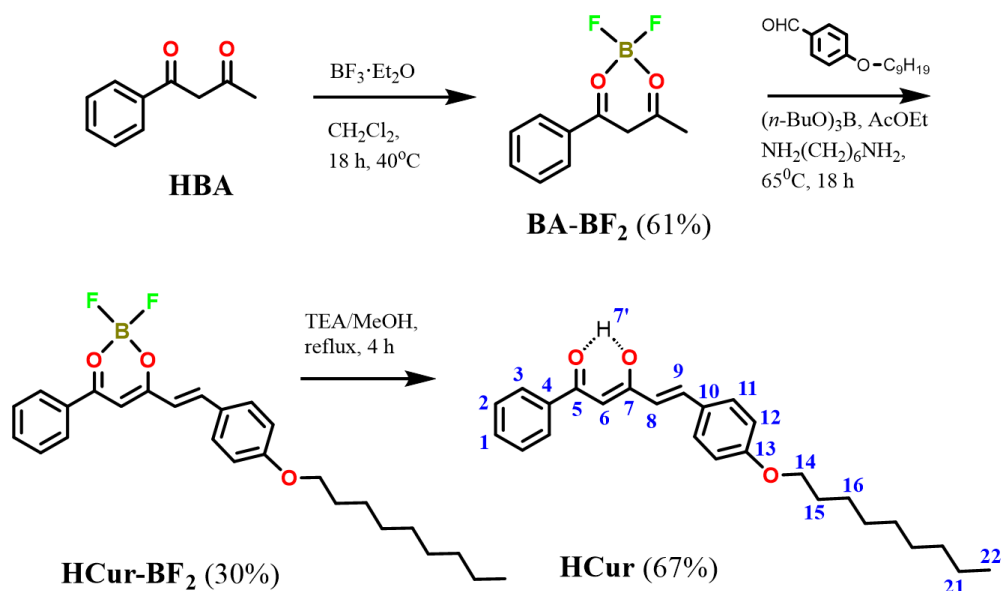
Copyright: © 2023 by the authors. Licensee MDPI, Basel, Switzerland. This article is an open access article distributed under the terms and conditions of the Creative Commons Attribution (CC BY) license (<https://creativecommons.org/licenses/by/4.0/>).

1. Introduction

The supramolecular assembly of different amphiphilic molecules allows for the incorporating of sensors into vesicular aggregates with high colloid stability and biocompatibility, which provides a good basis for creating sensory systems [1–5]. The uses of colorimetric and luminescence techniques for sensing are particularly attractive since they can facilitate the naked-eye or simple spectroscopic detection of biomolecules or water-soluble toxicants [6–11]. The development of sensory systems on the basis of supramolecular assemblies requires structure optimization on both molecular and supramolecular levels.

Curcumin and curcuminoid derivatives provide good basis for the development of sensors [12–17]. Moreover, synthetic modifications of curcuminoids and hemicurcuminoids allow an embedding of different functional groups into their molecules [18,19]. The resulting hemicurcumin **HCur** (also shown in Scheme 1) will be represented as a potential sensor

for the fluorescent monitoring of heavy metal ions and polyaminoacids. To overcome the poor water solubility of **HCur**, it has been incorporated into water-dispersible hydrophilic vesicular aggregates such as phospholipid vesicles and polydiacetylenic polymeric vesicular aggregates (PDAs), which are already documented as convenient nanoplatforms for the incorporation of luminophores, both organic [20] and complexed with metal ions [21–23].



Scheme 1. Synthetic sequence for the preparation of **HCur**.

It is well known that both the conformation and the electronic structure of dye molecules inserted into phospholipid vesicles are greatly influenced by their environment, which causes the sensitivity of dye molecules' phase transitions of phospholipid bilayers [24]. Moreover, both the conformational flexibility and hydrophobic or hydrophilic environment of a dye molecule have a major influence on its sensory function. Therefore, the inclusion of **HCur** molecules into mixed vesicular aggregates having both surface groups capable of pH-dependent ionization and a hydrophobic bilayer would provide a convenient basis for designing sensor systems focusing on the binding of both heavy metal ions and polylysine.

It is also worth noting that 10,12-pentacosadiynoic acid molecules are able to form polymeric polydiacetylene (PDA) nanoparticles after their self-organization into bilayers and subsequent polymerization [25,26]. Moreover, the relationship between the protonation/deprotonation of the surface-exposed carboxylic groups of PDA and ordering/disordering within their hydrophobic ene-yne conjugation backbone [27–30] is the already-documented reason for the colorimetric response to the binding event [31–33]. The interplay between fluorescent and colorimetric responses of **HCur** molecules and PDA vesicles, respectively, will also be demonstrated as a tool to alter the sensory functions of mixed **HCur**-PDA vesicles. The present work is aimed at using the assembly of **HCur** molecules with phospholipids or 10,12-pentacosadiynoic acid (a monomeric unit of PDA polymer vesicles) as a tool for tuning the conformation and electronic structure of **HCur** for the modification of its sensory function.

2. Experimental Section

2.1. Reagents and Materials

AcOEt (Acros Organics) was distilled over P_2O_5 . $\text{DMSO-}d_6$ (99.5% isotopic purity) from Aldrich was used for NMR spectroscopy. Methanol (99.9%), 1-benzoylacetone (**HBA**), 4-hydroxybenzaldehyde, triethylamine (TEA), $\text{BF}_3 \cdot \text{Et}_2\text{O}$ (48%), and 1,6-diaminohexane (Acros Organics) were used as commercially received without further purification.

Compounds 10,12-pentacosadiynoic acid, L- α -Phosphatidylcholine (P3644, $M_{av} = 776$ g/mol), 1,2-Diacyl-sn-glycero-3-phospho-L-serine (P7769, $M_{av} = 790$ g/mol) were received from Sigma Aldrich.

Synthesis: The synthetic routes, structural formulae and numbering of atoms of the investigated compounds are shown in Scheme 1. The 4-nonyloxybenzaldehyde and benzoylacetone-difluoroboron (**BA-BF₂**) were obtained as described in the literature [34,35]. ¹H and ¹³C chemical shifts and spin-spin coupling constants observed for synthesized hemicurcuminoids **HCur-BF₂** and **HCur** are presented in Table S1. **HCur** was characterized by high resolution mass spectrometry (HRMS) data (Figure S1).

Synthesis of **HCur** was performed through the preliminary synthesis of **HCur-BF₂** (the detailed synthetic procedure is in the Supplementary Materials) followed by its hydrolysis with the production of **HCur** (the detailed procedure is in the Supplementary Materials).

2.2. Synthesis of the Mixed Vesicles

HCur-PC(PS). The L- α -Phosphatidylcholine (PC), 1,2-Diacyl-sn-glycero-3-phospho-L-serine (PS) and **HCur** were dissolved in chloroform. Aliquots of **HCur** (0.314 mL, 0.26 mM) and PC (2.0 mL, 2.58 mM) or PS (2 mL, 2.53 mM) were mixed and evaporated at 40 °C and \approx 450 mbar. De-ionized water (16 mL) was added to the thin film, and the resulting solution (0.32 mM PC/PS with 0.05 mM of **HCur**) was sonicated in an ultrasonic bath for 4 min at 25 °C. Vesicles **HCur-PC** and **HCur-PS** were used as is after the synthesis.

HCur-PDA. The synthesis of **HCur:PDA**s were in accordance with the previously published procedure [36]. The monomeric 10,12-tricosadiynoic acid was dissolved in chloroform and filtered by using a 0.45 μ m nylon filter to remove polymerized particles. Aliquots of 10,12-PCDA (1.87 mL, 4.27 mM) and **HCur** (0.314 mL, 0.26 mM) were mixed and evaporated at 40 °C and \approx 450 mbar. De-ionized water (16 mL) was added to the thin film, and the resulting solution (0.5 mM PCDA with 0.05 mM of **HCur**) was sonicated in an ultrasonic bath for 4 min at 60 °C. Vesicles were stored at 4 °C within 24 h, and then were polymerized in a Petri dish using UV Crosslinker Bio-link 254 for 60 s.

The molar ratios of **HCur:PC**, **HCur:PS** and **HCur:PDA** were determined through the spectral analysis of the residual amounts of **HCur** after the thin film step according to the procedure described in Supplementary Materials. The molar ratios were calculated through Equation (1) represented in the Supplementary Materials

2.3. Methods

The detailed descriptions of common methods such as C, H microanalysis, mass spectra, high resolution mass spectra, dynamic light scattering (DLS), conditions and equipment for electronic absorption and fluorescence spectra measurements, and pH-measurements are presented in the Supplementary Materials.

The equipment for collecting of X-ray diffraction data is described in the Supplementary Materials. The collection and treatment of the data was conducted on the basis of well-known techniques and programs [37–41]. Crystallographic data (excluding structure factors) for the investigated structure **3** has been deposited in the Cambridge Crystallographic Data Centre as supplementary publication no. CCDC 2213569. Copies of the data can be obtained free of charge upon application to the CCDC (12 Union Road, Cambridge CB2 1EZ UK. Fax: (internat.) +44-1223/336-033; E-mail: deposit@ccdc.cam.ac.uk).

2.4. Computations

The thermodynamically correct structural ensembles for the conformers of each possible tautomer of **HCur** were generated with the use of CREST (short for Conformer-Rotamer Ensemble Sampling Tool) program [42]. Free energies of the generated species in solutions were calculated with the recently published CENSO protocol of Grimme et al. [43], designed for the evaluation of structure ensembles containing non-rigid molecules. The geometries were optimized with the r²SCAN-3c [44] composite density functional in their respective solutions using the DCOSMO-RS [45] implicit solvation model, whereby interactions

with the environment are already considered from the beginning. Solvation contributions δG_{solv} to the free energy at 298.15 K were obtained with COSMO-RS [46,47] using the *BP_TZVP_C30_1601.ctd* parameterization in combination with the energy and density of the high-level single-point calculation. The thermostistical contributions to the free energy were obtained by single-point hessian (SPH) calculations [48] within the framework of the modified rigid-rotor-harmonic-oscillator statistical treatment (ΔG_{mRRHO}) [49,50] at the GFN2-xTB [51] /ALPB [52] level, where GFN2-xTB is the robust and fast semi-empirical quantum chemical method and ALPB is the robust and efficient implicit solvation model for fast semiempirical methods. The final free energies were obtained from $\Delta G = \Delta E(\text{r}^2\text{SCAN-3c}) + \Delta G_{\text{mRRHO}}(\text{GFN2-xTB/ALPB}) + \Delta \delta G_{\text{solv}}(\text{COSMO-RS})$.

The most stable conformers of each tautomer, revealed on the basis of computed ΔG values, were used in the computation of UV-Vis spectra. Time-dependent density functional response theory (TD-DFT) [53–55] has been employed to compute the vertical excitation energy (i.e., absorption wavelengths) and oscillator strength on the ground state geometries optimized within the framework of the CENSO protocol as described above. For this purpose, the PBE0 function [56] in combination with the Ahlrichs' triple- ζ def2-TZVP AO basis set [57–59] was used.

The same conformers were further used as starting structures to generate clusters of these species explicitly solvated by PC or PCDA molecules. Clusters are generated by the *Quantum Cluster Growth* (QCG) algorithm [60,61] which, in short, adds solvent molecules around the solute at energetically favorable positions using an intermolecular force field docking algorithm (xTB-IFF) [20]. The cluster-generation step is followed by molecular dynamics (MD) simulations with the use of the recently developed general force field GFN-FF [62]. Equilibrated snapshots from the trajectory are fully geometry-optimized at the GFN2-xTB level, forming an ensemble of low-energy clusters. The dynamical behavior of the clusters of the lowest free energy (i.e., including thermostistical corrections) was further studied within the framework of the MD approach. MD trajectories of 1200 ps were carried out with the use of a generic all-atomic force field GFN-FF. All DFT and TD-DFT calculations were carried out using the Turbomole-7.5.1 program package [63].

3. Results and Discussion

3.1. Synthesis and Structure of Hemicurcuminoids

The synthesis of the hemicurcuminoid **HCur-BF₂** was carried out by the condensing of 4-nonyloxy-benzaldehyde with the boric complex of benzoylacetone (**BA-BF₂**) (Scheme 1). Aldol condensation and the subsequent destruction of the boron complex, achieved by its treatment of boiling in MeOH with the addition of TEA in the case of **HCur-BF₂**, leads to the formation of target hemicurcuminoid (**HCur**). The obtained compounds were characterized by the elemental analyses, NMR and MS techniques. According to ¹H NMR data, the compound **HCur** in DMSO-*d*₆ solution at a concentration of 0.03 M is found in enol form (>99%).

The structure of **HCur** was finally established by a single crystal X-ray crystallography of the separated crystal grown from the DMSO-*d*₆ (Figure 1a). Compound **HCur** belongs to the monoclinic system, space group *C2/c* (Table S2). The crystal consists only of hemicurcuminoid **3** molecules, which are in enol form as well as in DMSO-*d*₆ solution. This form is stabilized by intramolecular hydrogen bonds between the hydrogen atom of the hydroxyl group and the oxygen atom of the carboxyl group [O3-H3...O1 (2.4736(15) Å)] (Figure 1b). In general, the molecule has a flat elongated structure where all carbon atoms are practically in the same plane (Figure 1c). This fact can be explained by the conjugation effect in the molecule and the effect of packing.

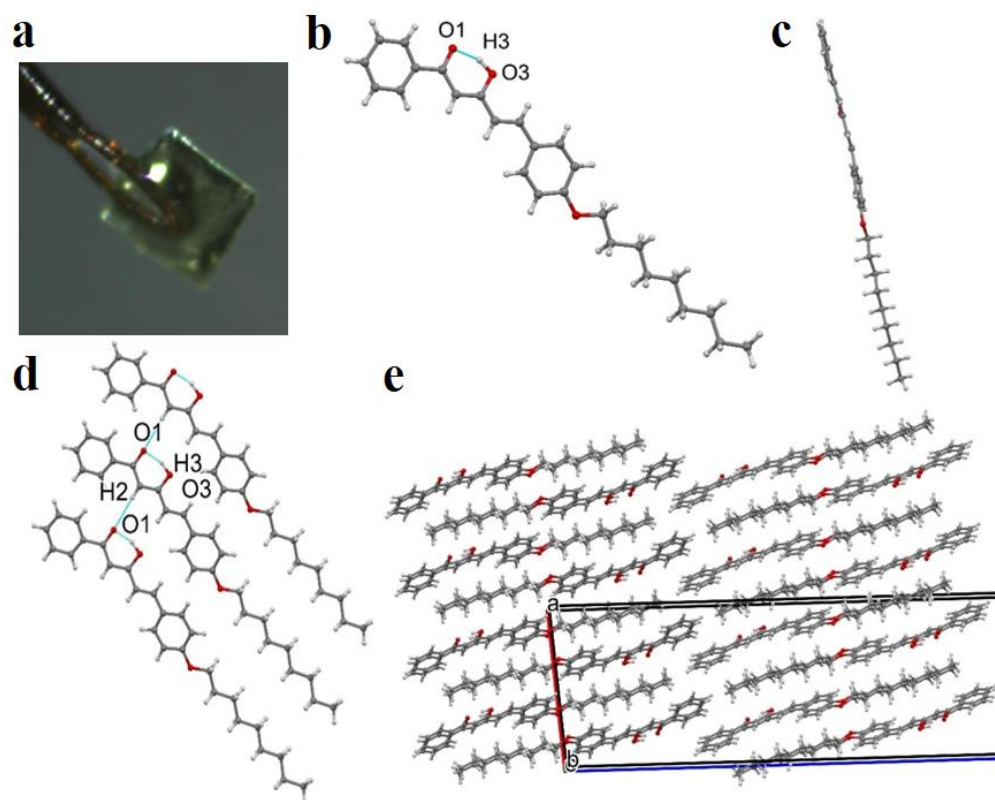


Figure 1. (a) Photo of the single crystal of **HCur**; (b,c) ORTEP view of two projections of the molecule in the crystal. Non-hydrogen atoms are represented by probability ellipsoids of thermal vibrations ($p = 50\%$), hydrogen atoms by spheres of arbitrary radii. (d) O-H ... O and C-H ... O hydrogen bonds (blue dashed lines) in the crystal **3**; (e) molecular packing fragment in the crystal **3**, hydrogen atoms are not shown for clarity.

An intermolecular hydrogen bond was observed between the hydrogen atom of the hydroxy group and the oxygen atom of the carbonyl group [C2-H2...O1 (2.690(17) Å, symmetry code: $x, -1+y, z$)] (Figure 1d). This hydrogen bond forms a chain structure along the b -axis. A molecular packing diagram of **HCur** is shown in Figure 1e and represents an antiparallel stacking of H-chains along the a -axis mainly through the van der Waals interactions. Although such packing leads to the absence of voids in the crystal, it does not lead to the densest packing, since the calculated packing factor of Kitaygorodsky is equal to 0.699, which is in the middle part of the range characteristic for crystals of organic compounds (0.65–0.75). At the same time, despite the planar conformation, these molecules turn out to be sufficiently labile for the formation of various types of crystal packings, as evidenced by our obtaining crystals of this compound of a different triclinic modification. Research on these crystals is ongoing.

3.2. Synthesis and Spectral Properties of PDA-HCur, PC-HCur, PS-HCur

The amphiphilic nature of **HCur** (its structure is shown in Scheme 1) is the reason for its incorporation into the PC-, PS- and PCDA-based vesicles. The nonyl substituents of the **HCur** molecules provide the driving force of their incorporation into PC-, PS- and PCDA-based vesicles through the well-known hydrophobic effect, resulting in the mixed vesicles' formation. The mixed vesicles were synthesized through the modified thin-film synthetic procedure described in detail in the Exp. Section. The synthesis was performed at various **HCur**:PCDA molar ratios, followed by analysis of residual amounts of **HCur** after the exposure of the mixed thin film (PCDA-**HCur**) to an aqueous solution under ultrasonication. The residual amounts of **HCur** were evaluated by spectrophotometry after their dissolution in chloroform (more details are in the Supplementary Materials,

Figure S2). These results allow the optimization of the synthetic procedure and calculation of the **HCur**:PCDA molar ratio (1:45) in the mixed vesicles. A similar synthetic strategy was applied in the synthesis of the mixed PC- and PS-based vesicles. The analysis of the residual amounts of **HCur** also confirms its incorporation into the PC- and PS-based vesicular aggregates, although the calculated **HCur**:PC(PS) molar ratios are 1:12 and 1:14, correspondingly. The incorporation of **HCur** molecules into the phospholipid vesicles is manifested by the electronic absorption bands shown in Figure 2a. Contributing to the spectral profile of **HCur**-PDA is the intensive bands at 560–640 nm arising from the ene-yne conjugation backbone of the PDA nanoplatform, while the electronic absorption of **HCur** in **HCur**-PDA is blue-shifted vs. **HCur**-PC(PS) (Figure 2a). The poor photobleaching of **HCur** under the irradiation required for the photopolymerization (Figure S2) prerequisites the conversion of **HCur**-PCDA vesicles into **HCur**-PDA polymeric ones without the significant photodegradation of **HCur** molecules.

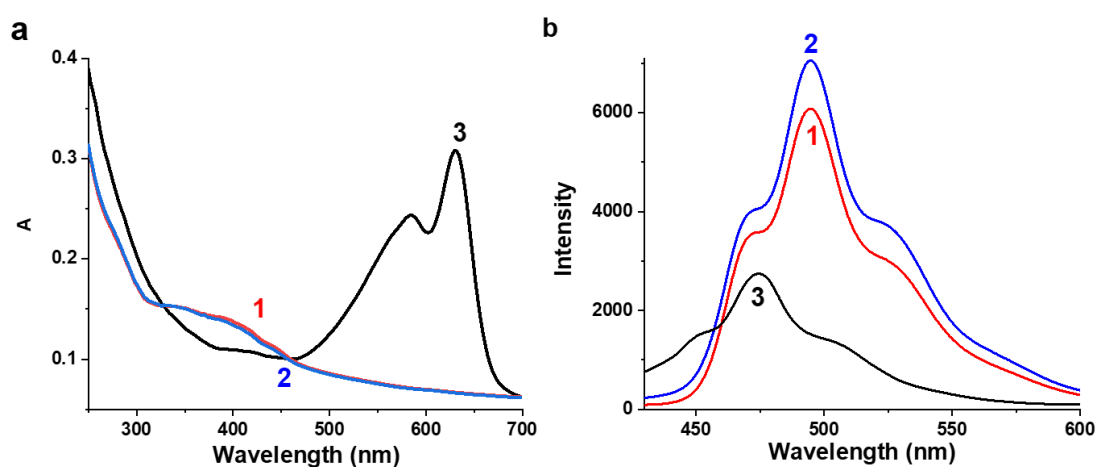


Figure 2. Electronic absorption (a) and emission spectra (b) of **HCur**-PC ($C_{\text{HCur}} = 0.041$), **HCur**-PS ($C_{\text{HCur}} = 0.036$) and **HCur**-PDA ($C_{\text{HCur}} = 0.011$).

The electronic absorption and emission spectral profiles of **HCur** are greatly affected by the nature of the nanoplatform (Figure 2), although the represented spectra differ from those performed in chloroform and DMF solutions (Figure S3). The main difference is the increased intensity of the longer wavelength emission, which shifts the maximum from 471 nm in DMF to 494–500 nm in PC and PS vesicles, while the emission at 470–475 nm still remains as the shoulder in the spectra along with the appearance of the shoulder at ~570 nm (Figures 3b and S3). The spectra of **HCur** incorporated into PDA vesicles have a maximum at ~480 nm, while the emission at ~510 and ~555 nm is manifested by the shoulders (Figure 2b). It is worth discussing the main factors affecting the emissive properties of **HCur** molecules in the mixed vesicles, since the properties are dependent on the nature of the nanoplatform.

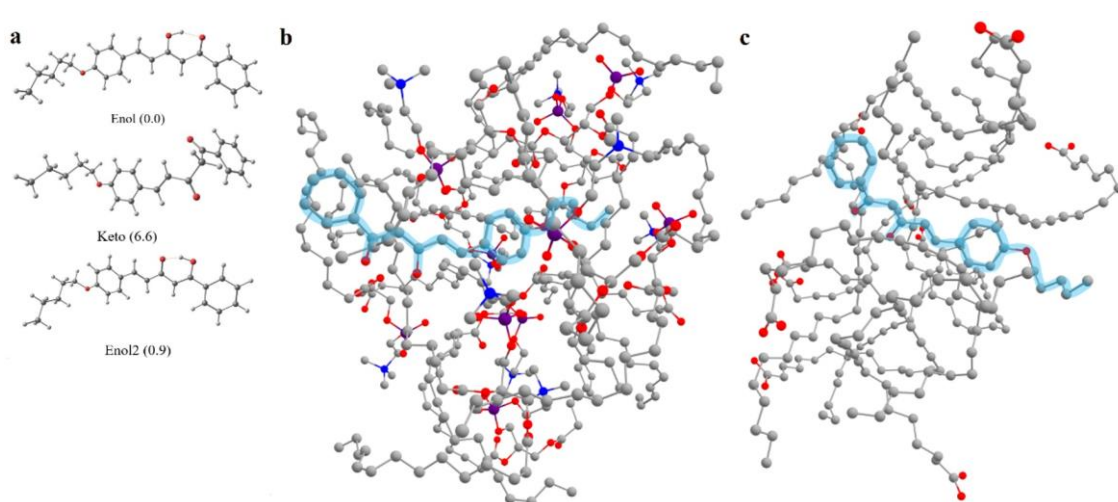


Figure 3. (a) Structures of the most energetically stable conformers of the simplified model of **HCur** and their relative Gibbs free energies ($\Delta G/\text{kcal}\cdot\text{mol}^{-1}$, in parentheses) computed with the use of CENSO protocol for chloroform solution. (b,c) Optimized structures of cluster **HCur-PC** and **HCur-PCDA** obtained by MD simulation, where hydrogen atoms are omitted for clarity.

The keto-enol tautomeric equilibrium shift is the main factor influencing the luminescence of curcuminoid derivatives [64]. The computations were performed in order to reveal which tautomeric form of **HCur** is most favorable in their mixed aggregates with PC molecules. Three possible tautomers of the simplified model of **HCur** are shown in Figure 3. According to the free energy values computed for molecules implicitly solvated by dimethylformamide or chloroform, enol tautomer strongly dominates in both media. It should be noted that the same form is also found in single crystals of **HCur** (cf. Figures 1b and 3a). UV-Vis spectra were simulated for the most stable conformers of each tautomer (Figure 3a), revealed on the basis of their computed free energies. The TD-DFT simulated spectrum of keto tautomer contains two strong bands in the spectral interval $\sim 300\text{--}450$ nm, while only one band at ~ 390 nm is registered in the UV-Vis spectra of solutions. The latter band is fairly well matched by the only strong band (~ 400 nm) in this interval, which is computationally predicted for enol and enol2 tautomers. The experimental absorption spectra of **HCur-PC** and **HCur-PCDA** in the spectral interval $\sim 300\text{--}450$ nm are very similar to the spectra of solutions discussed above, which strongly suggests that enol tautomers are the major forms of **HCur** in all systems under study.

For the above reason, computational modeling of the structural arrangement of **HCur-PC** and **HCur-PCDA** aggregates was conducted for the single enol tautomer of **HCur** surrounded by (a) ten PC or (b) ten PCDA molecules in the aqueous environment modeled implicitly. According to our computations of system (a), Ph(C=O) moiety of **HCur** is pushed to the periphery of the cluster (Figure 3b) and almost completely immersed in the surrounding water shell. The molecule of the dye is situated in a rather narrow well, formed mainly by long hydrocarbon tails of PC. In contrast, in the case of system (b), PCDA molecules form a rather loose disk-like association, and the dye molecule penetrates into it in such a way that both its Ph(C=O) head and its long tail protrude into the surrounding water from opposite sides of the cluster (Figure 3c), and the entire surface of **HCur** is only weakly screened by PCDA molecules.

Thus, the enolic form of **HCur** predominates in the mixed vesicles, although the location of **HCur** molecules within the PC- and PCDA-based bilayers is quite different, which is reflected, e.g., in different exposures of the molecules to the hydrated exterior layer. This can be a reason for the different spectral patterns of **HCur** in the PDA- and PC(PS)-based vesicles, although possible translocations of **HCur** molecules within the PDA-bilayer during photopolymerization of **HCur-PCDA** vesicles cannot be excluded. Moreover, the experimentally observed smaller loading extent of **HCur** into PDA- in comparison with

PC(PS)-based vesicles agrees with the MD calculations revealing better compatibility of **HCur** with the phospholipids than with PCDA molecules reflected in more close contact of the dye with the former matrix than with the latter environment.

The planarity of **HCur** molecules can be distorted when their R-substituents are incorporated into the hydrophobic layer of the vesicles, which may blue-shift the emission bands. The deprotonation of the enolic form of curcumine and curcuminoid derivatives is another reason for the changes in their emissive properties [65]. The phase transitions in the mixed bilayers should also be mentioned as the factor triggering a translocation of the dye molecules from the hydrophobic core of the PhL bilayers to their polar periphery, typically manifested by the changes in the dye spectra [66,67]. Finally, the aggregation of mixed vesicles can be considered as another factor affecting the luminescence of the **HCur** molecules included into the vesicular aggregates.

The incorporation of the dye molecules into the phospholipid vesicles is the reason for the disturbing of the structural ordering in their hydrophobic layers, which can be followed by the enhanced aggregation of the mixed vesicles vs. their pure phospholipid counterparts [68]. The DLS data (Figure 4) measured for the aqueous solutions of the mixed vesicles reveal the average size values, which are greater than the previously reported values of the PC and PDA vesicles [69] and those of the PS vesicles measured in similar conditions (Figure S4). The size and polydispersity characteristics calculated from the DLS data (Table 1) indicate that the incorporation of **HCur** molecules into the PC-, PS- and PDA-based bilayers affects the size and stability of the mixed vesicular aggregates but does not cause significant aggregation of the mixed vesicles.

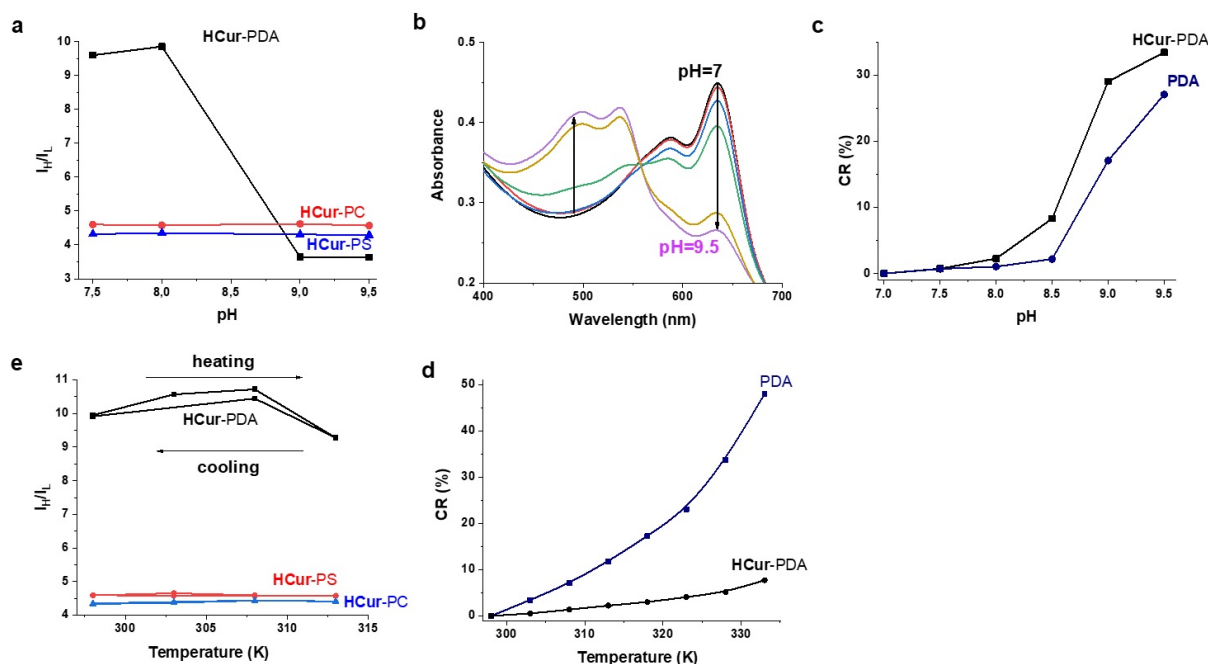


Figure 4. (a) I_H/I_L of **HCur-PC**, **HCur-PS** and **HCur-PDA** at different pH values; (b) UV-vis spectra of **HCur-PDA** at different pH; (c) colorimetric response of **HCur-PDA** and **PDA** at different pH; (d) colorimetric response of **HCur-PDA** and **PDA** at different temperature (T, K); (e) I_H/I_L of **HCur-PC**, **HCur-PS** and **HCur-PDA** at different T.

Table 1. Size distribution by volume and intensity of **HCur-PC** (1), **HCur-PS** (2) and **HCur-PDA** (3) at pH = 8.1.

	PdI	Size by Intensity (d_I , nm)	Size by Volume (d_V , nm)
HCur-PC	0.430	47 ± 8 265 ± 88	43 ± 9 274 ± 99
HCur-PS	0.594	125 ± 63	66 ± 49
HCur-PDA	0.450	271 ± 100	283 ± 115

3.3. Dependence of Spectral Behavior of PDA-HCur, PC-HCur, PS-HCur on External Stimuli (pH, Heating, Metal Ions)

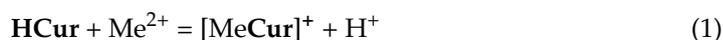
The enolic forms of **HCur** molecules can undergo dissociation in specific pH conditions, followed by the enhancement of the lower energy emission [65]. The lack of detectable changes in the ratios of the intensities of the lower and higher energy transitions of **HCur-PDA** or **HCur-PC(PS)** vesicles under the acidification of their aqueous dispersions to pH values below 7.5 (Figure S5a–c) indicates the insignificant deprotonation of **HCur** molecules in the aforesaid conditions.

The pH-dependence of the emission was analyzed through the intensity ratios measured for higher- and lower-energy bands (I_h/I_l) at 474 and 555 nm, respectively, for **HCur-PDA**, and at 495 and 555 nm, respectively, for **HCur-PC(PS)**. The I_h/I_l values at various pHs are plotted in Figure 4a. The results represented in Figure 4a indicate the insignificant changes under the alkalization of **HCur-PC(PS)** aqueous colloids to a pH above 8.5, while the ratios measured for **HCur-PDA** decrease under the alkalization. Similar to the PDA-vesicles themselves [70], the alkalization to pHs above 7.5 triggers the chromatic changes (Figure 4b) peculiar for the blue-to-red transitions of PDA vesicles. It has been already documented that the incorporation of the amphiphilic molecules into the PDA vesicles can stabilize either red [71] or blue forms [36] of the PDA-based backbones. The comparative monitoring of the pH-induced colorimetric changes of **HCur-PDA** and PDA vesicles through the CR% (Colorimetric Response calculated by the Equation (2) in the Supplementary Materials) indicate that both vesicles exhibit the blue-to-red transition at pHs above 8.0, while the transition of **HCur-PDA** becomes detectable at pH > 8.0 and while greater alkalization is required for the similar transition of PDA vesicles (Figures 4c and S4d).

Heating is another well-known trigger of the blue-to-red transition [72]. Thus, the heating-induced changes of **HCur-PDA** vesicles should be compared with those of PDA itself. The data presented in Figure 4d indicate very poor transitions up to 55 °C, while the PDA vesicles themselves exhibit significant blue-to-red transition in these conditions.

The fluorescence of **HCur** in the phospholipid vesicles exhibits insignificant changes in the I_h/I_l values under heating (Figure 4e), while changes are detectable under the heating of **HCur-PDA** vesicles. The aforesaid changes can be correlated with the temperature-dependence of both conformational changes of **HCur** in the PDA-vesicles and hydration-induced quenching. Thus, the greater distortions of **HCur** molecules under their incorporation into the PDA-vesicles vs. the PC(PS)-vesicles correlate with the higher sensitivity of **HCur-PDA** in comparison with **HCur-PC(PS)** to the temperature changes.

Coordinative bonds can provide a good basis for the spectral response of **HCur** incorporated into the vesicular aggregates. It is worth noting that the enolic form of **HCur** can coordinate metal ions (Me^{2+}) in accordance with the equilibrium (1)



However, the spectral response of **HCur** to heavy metal ions is negligible in **HCur-PC** and small in **HCur-PS** (Figure S5), but becomes significant for **HCur-PDA** (Figure 5a,b). This agrees well with the above-mentioned difference in the location of **HCur** molecules within the PC- and PCDA-based bilayers. The concentration-dependent quenching of both

the higher (474 nm) and lower (555 nm) energy bands of **HCur**-PDA observed under the increase in concentrations of Co^{2+} , Mn^{2+} , Ni^{2+} (Figure S6) results from their coordination with the enolate form of **HCur** (Figure S6). The luminescent response of **HCur**-PDA to the growing amounts of Cd^{2+} and Pb^{2+} is manifested by both enhancement of the lower energy and quenching of the higher energy bands (Figure 5a,b). The peculiarity of the luminescent response of **HCur**-PDA to Cd^{2+} and Pb^{2+} ions is demonstrated by the $I_{\text{h}}/I_{\text{l}}$ values (Figure 5c). The values remain practically unchanged in the wide concentration range of Co^{2+} , Mn^{2+} , Ni^{2+} , while the concentration-dependent decrease of $I_{\text{h}}/I_{\text{l}}$ values is observed in the solutions of Cd^{2+} and Pb^{2+} (Figure 5c). The aforesaid peculiarity derives from the increased planarity of the **HCur** molecule under the complex formation with Pb^{2+} and Cd^{2+} . Moreover, the $I_{\text{h}}/I_{\text{l}}$ values plotted vs. various concentrations of metal ions reveals the selectivity of the **HCur**-PDA sensor to Cd^{2+} over Pb^{2+} ions (Figure 5c). It is worth noting that the selectivity derives from the conformational changes of **HCur** resulting from its complex formation with Cd^{2+} and Pb^{2+} ions with specific electronic structure (d^{10} and $d^{10}s^2$ correspondingly). Thus, both nature and lengths of coordination bonds are worth noting among the factors influencing such changes, although all the factors responsible for the sensitivity cannot be specified within the present work scope.

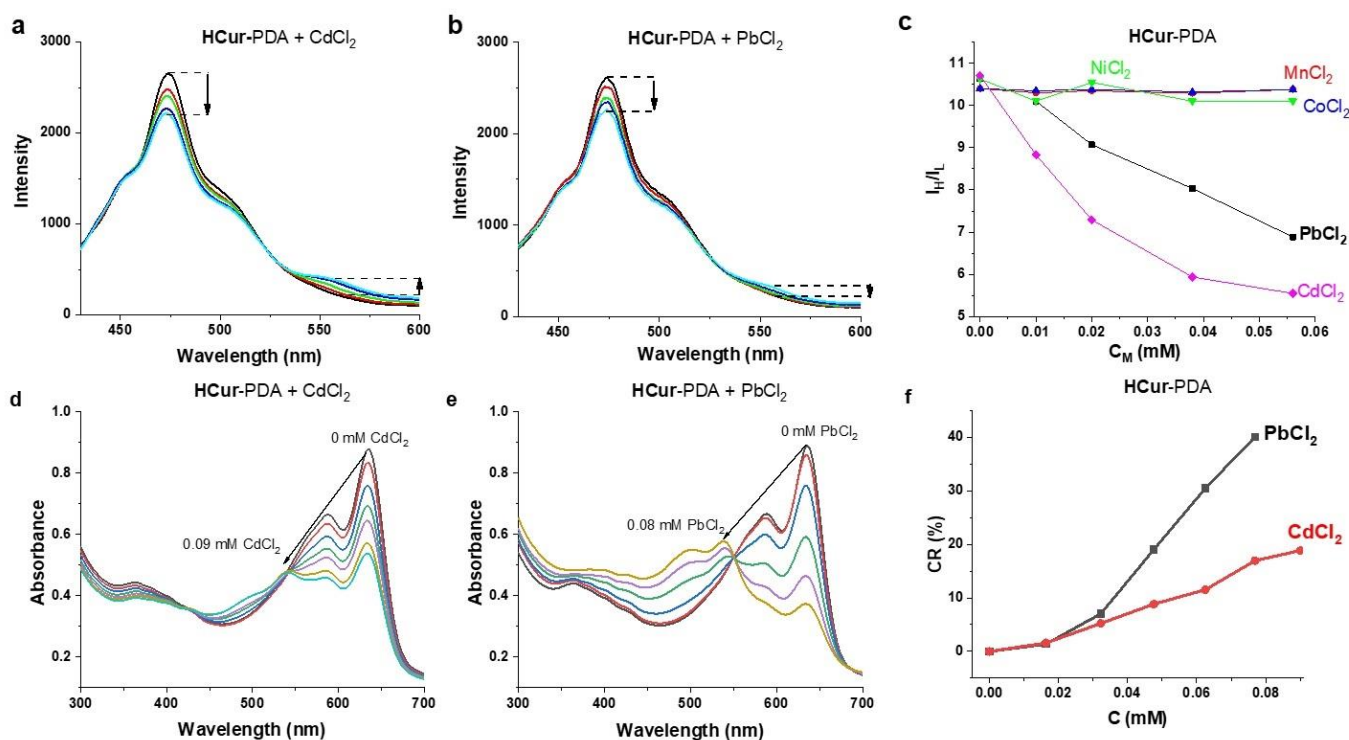


Figure 5. (a,b) Luminescence spectra of **HCur**-PDA at the concentration of CdCl_2 and PbCl_2 varied from 0 to 0.058 mM (pH = 7.5). (c) $I_{\text{h}}/I_{\text{l}}$ of **HCur**-PDA vs. concentration of d-metal cations (pH = 7.5): CdCl_2 ; PbCl_2 ; NiCl_2 ; MnCl_2 ; CoCl_2 . (d,e) UV-vis spectra of **HCur**-PDA at pH = 7.5 and different concentration of CdCl_2 (d) and PbCl_2 (e). (f) Colorimetric response (CR%) of **HCur**-PDA to CdCl_2 and PbCl_2 .

It is well known that the coordinative binding with Pb^{2+} ions facilitates the blue-to-red transition of the PDA vesicles modified by the additional ligands [73–76]. The monitoring of the electronic absorption spectra of the **HCur**-PDA vesicles under the growing concentrations of Pb^{2+} and Cd^{2+} (Figure 5d,e) indicates the specific colorimetric response of **HCur**-PDA to Pb^{2+} and Cd^{2+} ions (blue-to-red transition).

Thus, the aforesaid reveals **HCur**-PDA vesicles as the more sensitive and selective nanosensor to metal ions than **HCur**-PC(PS) vesicles. This correlates with a higher exposure of **HCur** molecules to water in their supramolecular assemblies with PCDA molecules in

comparison with the **HCur-PC** assemblies revealed by our computational modeling (vide supra). Moreover, the **HCur-PDA** vesicles demonstrate both fluorescent and colorimetric responses to the heavy metal ions, although there is no correlation between I_H/I_L and CR% values (Figure 5f). In particular, the CR% values can distinguish between Pb^{2+} and Cd^{2+} ions at concentrations above 0.03 mM, while the I_H/I_L values give the selective response to Cd^{2+} over Pb^{2+} ions at concentrations below 0.01 mM. The different selectivity of the chromatic (Pb^{2+}) and fluorescent (Cd^{2+}) responses of **HCur-PDA** indicates that the latter derives from the complexation of the metal ions with **HCur**, while the former is predominantly affected by the complexation with the PDA platform.

3.4. Sensitivity of PDA-**HCur** Fluorescence to Polyaminoacids and Proteins

The presence of the multiple-surface exposed carboxy/carboxylate groups makes the PDA nanoplatform a convenient basis for the binding of macromolecules through the combined effect of electrostatic attraction and hydrogen bonding. Polylysine (PL) is a good choice to reveal an impact of the latter effect on both colorimetric and fluorescent responses of **HCur-PC(PS)** and **HCur-PDA** vesicular aggregates. PL molecules are well known for their conformational flexibility, being predominantly in α -helical structure at pHs above 10.4 and converting into the coil-like and β -sheet secondary structures at pHs below 8.0 [77]. The spectral response of **HCur-PDA** monitored in a buffer solution at pH 7.5 is evident from both fluorescent and chromatic changes under the increased concentration of PL (Figure 6a,b), which are manifested by the decrease in the I_H/I_L values and the increase in the CR values correspondingly (Figures 6c,d and S7c). It is worth noting that no significant changes in the I_H/I_L values are revealed for **HCur-PC(PS)** under the increased concentration of PL (Figures 6c and S7a,b).

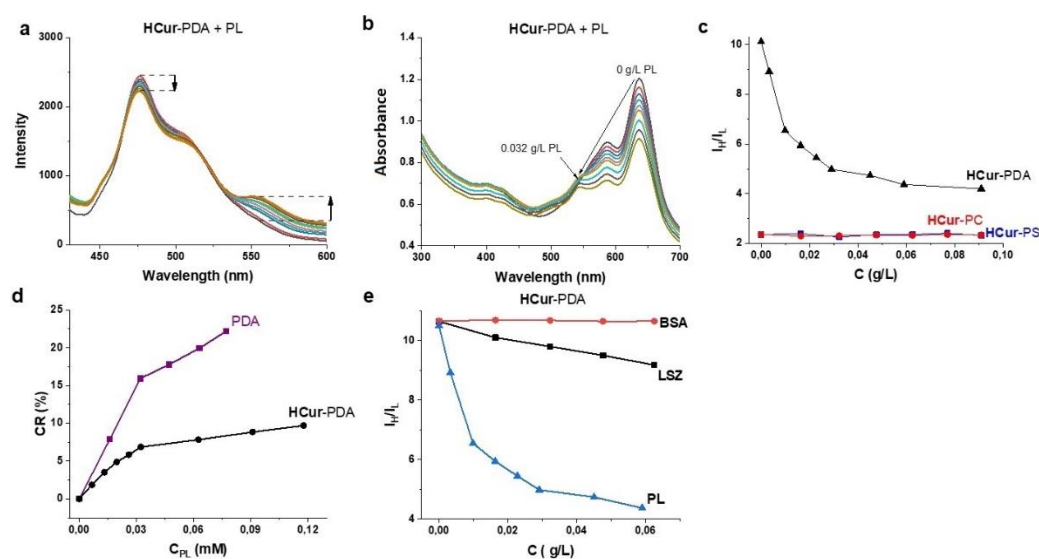


Figure 6. Luminescence (a) and electronic absorption spectra (b) of **HCur-PDA** at different concentrations of PL (from 0 to 0.091 g/L). (c) I_H/I_L of **HCur-PC**, **HCur-PS** and **HCur-PDA** vs. concentration of PL (from 0 to 0.091 g/L). (d) Colorimetric response of PDA and **HCur-PDA** to different concentrations of PL. (e) I_H/I_L of **HCur-PDA** at different concentration of PL, LSZ and BSA.

Thus, similarly to the above-mentioned spectral responses of **HCur-PDA** vesicles to alkalization and $Pb(Cd)^{2+}$ ions, the spectral response to PL reveals the interference between the chromatic and fluorescent changes. In particular, the incorporation of **HCur** is the factor suppressing the chromatic response of **HCur-PDA** to PL in comparison with that of PDA itself (Figure 6d). However, the close-to-linear increase in the CR values covers the concentration range 0–0.04 mM (Figure 6d), while the sharp decrease of the I_H/I_L values within 0.002–0.025 mM of PL comes to the saturation level at 0.02–0.045 mM

(Figures 6e and S7d,e). The difference in the concentration ranges required for the chromatic and fluorescent responses of **HCur**-PDA reveals the difference between the binding of PL molecules with the fluorescent (**HCur**) and colorimetric (PDA) sensors. However, the I_h/I_l values of **HCur**-PDA exhibit some decrease under the concentration of PL above 0.045 mM, which correlates with the blue-to-red phase transition of the PDA nanobead triggered by the interaction with PL. This provides one more argument for the interference between the colorimetric and fluorescent responses of **HCur**-PDA to PL.

The results reveal an impact of the surface-exposed amino/ammonium groups of PL molecules on their efficient binding with **HCur**-PDA, which raises a question about a possibility of its fluorescent response to Lysozyme (LSZ) with the net charge at 8e and $pI = 10.33$ [78]. LSZ does not trigger the chromatic responses of both PDA and **HCur**-PDA vesicles (Figure S6f). The fluorescent response of **HCur**-PDA requires a greater concentration of LSZ in comparison with that of PL. This correlates with the smaller amount of the surface-exposed amino/ammonium groups of LSZ, while the lack of any detectable fluorescent response of **HCur**-PDA to bovine serum albumin (BSA) correlates with its charge (−18e) and pI characteristics (4.7), which are quite different from those of LSZ.

4. Conclusions

In summary, the newly synthesized representative of the hemicurcuminoid family bearing a nonyl substituent (**HCur**) forms the supramolecular assemblies with phosphatidylcholine, phosphatidylserine and poly10,12-pentacosadiynoic acid (PCDA) molecules, which allows for the obtaining of mixed vesicular aggregates containing the fluorescent **HCur** through the thin film procedure. The **HCur**-PCDA vesicles were converted into the polymeric ones through photopolymerization. The phospholipid-based vesicles demonstrate the high loading by **HCur** molecules, while the loading extent is much less for the PDA-based vesicles. This correlates with molecular modeling simulations revealing the more favorable encapsulation of **HCur** molecules via their nonyl substituents into the phospholipid-based assemblies, while the PCDA-based assembly provides less efficient screening of **HCur** molecules from the exterior water molecules.

The single-crystal XRD analysis revealed a high planarity of **HCur** molecules in the solid state, although the planarity distortion of **HCur** may have affected its spectral behavior in the mixed vesicles. The spectral behavior of **HCur** in the PDA-based aggregates differed from that in the phospholipid-based ones. In particular, the fluorescence of **HCur** in the PDA-based vesicles demonstrated much greater sensitivity to the external stimuli (temperature changing from 293 to 313 K and the pH increase from 7.5 to 9.5) than the fluorescence of **HCur**-PC(PS) vesicles. This highlights an impact of greater exposure of **HCur** to a bulk of solution on the sensitivity of its fluorescence to the external stimuli.

It is also worth noting that **HCur**-PDA is introduced as the dual fluorescent-chromatic nanosensor. The difference in the sensitivity and selectivity of the fluorescent and chromatic responses of **HCur**-PDA indicates that they are driven by the substrate–**HCur** and substrate–PDA interactions correspondingly. Thus, the fluorescent response of **HCur**-PDA vesicles to both heavy metal ions (Pb^{2+} and Cd^{2+}) and polylysine is more sensitive than the colorimetric response of the vesicles, although both responses interfere with each other. This highlights both the molecular structure of **HCur** and its supramolecular package into the different vesicular aggregates as the key factors responsible for the sensing ability towards the heavy metal ions and polylysine. However, further modifications on both molecular and supramolecular levels are required to develop a sensor able to recognize protein molecules.

Supplementary Materials: The following supporting information can be downloaded at: <https://www.mdpi.com/xxx/s1>: Table S1. ^1H and ^{13}C chemical shifts (ppm) and spin-spin coupling constants (Hz) observed for the enol form of compounds HCur-BF₂ and HCur in DMSO-d₆ at 303K; Table S2. Experimental crystallographic data for compound 3; Figure S1 HRMS (ESI) of HCur (C₂₆H₃₂O₃), m/z : 393.2420, $[\text{M}+\text{H}]^+$, calcd for C₂₆H₃₃O₃ 393.2424; Figure S2 a - UV-vis spectra of HCur at different concentration. b - I₄₀₀ of UV-vis spectra of HCur at different concentration. c - UV-vis spectra of residual amount of HCur after synthesis of PC-HCur, PS-HCur and PCDA-HCur. (d) - UV-vis spectra of HCur in CHCl₃ at different time of UV-irradiation (254nm); Figure S3 a,b - Emission and excitation spectra of HCur in DMF (emission 470 nm, excitation 390 nm). c,d - Emission and excitation spectra of HCur in CHCl₃ (emission 460 nm, excitation 340 nm); Figure S4 Size distribution by Volume (red line) and by intensity (black line) of PDA-HCur(a), PC-HCur (b) and PS-HCur (c): a,b,c - at pH = 8.1; d,e,f - at pH = 3.5. g,h,i - size distribution of bilayers aggregates of PC (g), PS(h) and PDA(i); Figure S5. Luminescence spectra of PC-HCur(a), PS-HCur(b) and PDA-HCur(c) at different pHs. d - UV-vis spectra of PDA at different pHs; Figure S6. Luminescence spectra of PDA-HCur in presence of different concentration of CuCl₂ (a), MnCl₂ (b) and NiCl₂ (c); Figure S7. Luminescence spectra of HCur-PC(a) ab HCur-PS(b) and HCur-PDA(3) vs concentration of PL. c - UV-vis spectra of PDA at different concentration of PL. d,e - Luminescence spectra of HCur-PDA at different concentration of BSA and LSZ.

Author Contributions: B.S.A.: formal analysis, investigation, data curation, writing—original draft, writing—review and editing, visualization. O.O.R.: formal analysis. S.N.P.: formal analysis, investigation. S.A.K.: conceptualization, methodology, validation, formal analysis, writing—original draft, writing—review and editing. A.T.G.: formal analysis, investigation. S.N.S.: formal analysis, investigation. V.V.S.: formal analysis, investigation. V.M.B.: formal analysis. O.G.S.: conceptualization, validation. A.R.M.: conceptualization, supervision, methodology, validation, formal analysis, data curation, writing—original draft, writing—review and editing. All authors have read and agreed to the published version of the manuscript.

Funding: This research was funded by the government assignment for FRC Kazan Scientific Center of RAS.

Acknowledgments: The authors gratefully acknowledge the Assigned Spectral-Analytical Center of FRC Kazan Scientific Center of RAS for providing the necessary facilities to carry out physical-chemical measurements.

Conflicts of Interest: The authors declare no conflict of interest.

References

1. Ananda, A.; Moreira, R.; Henry, J.; Chowdhury, M.; Cote, G.; Good, T. A bio-sensing strategy for the detection of prions in foods. *LWT—Food Sci. Technol.* **2005**, *38*, 849–858. [[CrossRef](#)]
2. Gal, N.; Morag, A.; Kolusheva, S.; Winter, R.; Landau, M.; Jelinek, R. Lipid Bilayers Significantly Modulate Cross-Fibrillation of Two Distinct Amyloidogenic Peptides. *J. Am. Chem. Soc.* **2013**, *135*, 13582–13589. [[CrossRef](#)]
3. Grabowska, I.; Sharma, N.; Vasilescu, A.; Iancu, M.; Badea, G.; Boukherroub, R.; Ogale, S.; Szunerits, S. Electrochemical Aptamer-Based Biosensors for the Detection of Cardiac Biomarkers. *ACS Omega* **2018**, *3*, 12010–12018. [[CrossRef](#)]
4. Healey, M.; Sivakumaran, M.; Platt, M. Rapid quantification of prion proteins using resistive pulse sensing. *Analyst* **2020**, *145*, 2595–2601. [[CrossRef](#)]
5. Wang, S.; Zhao, Z.; Haque, F.; Guo, P. Engineering of protein nanopores for sequencing, chemical or protein sensing and disease diagnosis. *Curr. Opin. Biotechnol.* **2018**, *51*, 80–89. [[CrossRef](#)]
6. Tyagi, A.; Liu, X.; Abidi, I.H.; Gao, Z.; Park, B.M.; Zeng, X.; Ou, X.; Cagang, A.A.; Zhuang, M.; Hossain, D.; et al. Modular functionalization of crystalline graphene by recombinant proteins: A nanoplatform for probing biomolecules. *Nanoscale* **2018**, *10*, 22572–22582. [[CrossRef](#)]
7. Pandey, S.P.; Awasthi, A.A.; Singh, P.K. Supramolecular tuning of thioflavin-T aggregation hosted by polystyrene sulfonate. *Phys. Chem. Chem. Phys.* **2021**, *23*, 14716–14724. [[CrossRef](#)] [[PubMed](#)]
8. Goshisht, M.K.; Tripathi, N. Fluorescence-based sensors as an emerging tool for anion detection: Mechanism, sensory materials and applications. *J. Mater. Chem. C* **2021**, *9*, 9820–9850. [[CrossRef](#)]
9. Sevim, S.; Sorrenti, A.; Franco, C.; Furukawa, S.; Pané, S.; Demello, A.J.; Puigmartí-Luis, J. Self-assembled materials and supramolecular chemistry within microfluidic environments: From common thermodynamic states to non-equilibrium structures. *Chem. Soc. Rev.* **2018**, *47*, 3788–3803. [[CrossRef](#)]
10. Albrecht, M. Supramolecular chemistry-general principles and selected examples from anion recognition and metallosupramolecular chemistry. *Naturwissenschaften* **2007**, *94*, 951–966. [[CrossRef](#)]

11. Barooah, N.; Mohanty, J.; Bhasikuttan, A.C. Cucurbituril-Based Supramolecular Assemblies: Prospective on Drug Delivery, Sensing, Separation, and Catalytic Applications. *Langmuir* **2022**, *38*, 6249–6264. [[CrossRef](#)] [[PubMed](#)]
12. Sánchez, M.; Aranda, F.J.; Teruel, J.A.; Ortiz, A. New pH-sensitive liposomes containing phosphatidylethanolamine and a bacterial dirhamnolipid. *Chem. Phys. Lipids* **2011**, *164*, 16–23. [[CrossRef](#)]
13. Hu, J.; Wang, Y.; Shao, T.; Lian, G.; Hu, K.; Liu, Y.; Zhou, M.; Wang, X.; Huang, L.; Meng, X.; et al. Simple and practical, highly sensitive and responsive recognition of cysteine: Design, synthesis and mechanism study of a novel curcumin fluorescent probe. *Arab. J. Chem.* **2022**, *15*, 104087. [[CrossRef](#)]
14. Wang, F.; Huang, W.; Zhang, Y.; Wang, M.; Sun, L.; Tang, B.; Wang, W. Determination of Protein by Fluorescence Enhancement of Curcumin in Lanthanum-Curcumin-Sodium Dodecyl Benzene Sulfonate-Protein System. *J. Fluoresc.* **2010**, *21*, 25–34. [[CrossRef](#)] [[PubMed](#)]
15. Ran, C.; Xu, X.; Raymond, S.B.; Ferrara, B.J.; Neal, K.; Bacskai, B.J.; Medarova, Z.; Moore, A. Design, Synthesis, and Testing of Difluoroboron-Derivatized Curcumins as Near-Infrared Probes for in Vivo Detection of Amyloid- β Deposits. *J. Am. Chem. Soc.* **2009**, *131*, 15257–15261. [[CrossRef](#)]
16. Khorasani, M.Y.; Langari, H.; Sany, S.B.T.; Rezayi, M.; Sahebkar, A. The role of curcumin and its derivatives in sensory applications. *Mater. Sci. Eng. C* **2019**, *103*, 109792. [[CrossRef](#)]
17. Zakaria, H.; El Kurdi, R.; Patra, D. Curcumin-PLGA based nanocapsule for the fluorescence spectroscopic detection of dopamine. *RSC Adv.* **2022**, *12*, 28245–28253. [[CrossRef](#)]
18. Priyadarsini, K.I. The Chemistry of Curcumin: From Extraction to Therapeutic Agent. *Molecules* **2014**, *19*, 20091–20112. [[CrossRef](#)]
19. Lyu, H.; Wang, D.; Cai, L.; Wang, D.-J.; Li, X.-M. Synthesis, photophysical and solvatochromic properties of diacetoxyboron complexes with curcumin derivatives. *Spectrochim. Acta Part A Mol. Biomol. Spectrosc.* **2019**, *220*, 117126. [[CrossRef](#)] [[PubMed](#)]
20. Reppy, M.A. Enhancing the Emission of Polydiacetylene Sensing Materials Through Fluorophore Addition and Energy Transfer. *J. Fluoresc.* **2008**, *18*, 461–471. [[CrossRef](#)]
21. Sansee, A.; Kamphan, A.; Traiphol, R.; Kielar, F. Embedding luminescent iridium complex into polydiacetylene vesicles as a means of development of responsive luminescent system for imaging applications. *Colloids Surfaces A Physicochem. Eng. Asp.* **2016**, *497*, 362–369. [[CrossRef](#)]
22. Jose, D.A.; Stadlbauer, S.; König, B. Polydiacetylene-Based Colorimetric Self-Assembled Vesicular Receptors for Biological Phosphate Ion Recognition. *Chem.—A Eur. J.* **2009**, *15*, 7404–7412. [[CrossRef](#)]
23. Mounica, A.; Balachandran, C.; Gopalakrishnan, D.; Sivasakthi, P.; Prakash, M.; Aoki, S.; Ganeshpandian, M. Synthesis and antiproliferative activity of novel organometallic cobalt(III) complex encapsulated in polydiacetylene-phospholipid nanoformulation. *Inorganica Chim. Acta* **2022**, *530*, 120701. [[CrossRef](#)]
24. Akhmadeev, B.; Gerasimova, T.; Gilfanova, A.; Katsyuba, S.; Islamova, L.; Fazleeva, G.; Kalinin, A.; Daminova, A.; Fedosimova, S.; Amerhanova, S.; et al. Temperature-sensitive emission of dialkylaminostyrylhetarene dyes and their incorporation into phospholipid aggregates: Applicability for thermal sensing and cellular uptake behavior. *Spectrochim. Acta Part A Mol. Biomol. Spectrosc.* **2022**, *268*, 120647. [[CrossRef](#)] [[PubMed](#)]
25. Chen, X.; Zhou, G.; Peng, X.; Yoon, J. Biosensors and chemosensors based on the optical responses of polydiacetylenes. *Chem. Soc. Rev.* **2012**, *41*, 4610–4630. [[CrossRef](#)] [[PubMed](#)]
26. Carpick, R.W.; Sasaki, D.Y.; Marcus, M.S.; Eriksson, M.A.; Burns, A.R. Polydiacetylene films: A review of recent investigations into chromogenic transitions and nanomechanical properties. *J. Phys. Condens. Matter* **2004**, *16*, R679–R697. [[CrossRef](#)]
27. Reppy, M.A.; Pindzola, B.A. Biosensing with polydiacetylene materials: Structures, optical properties and applications. *Chem. Commun.* **2007**, *42*, 4317–4338. [[CrossRef](#)]
28. Champaiboon, T.; Tumcharern, G.; Potisatituyenyong, A.; Wacharasindhu, S.; Sukwattanasinitt, M. A polydiacetylene multilayer film for naked eye detection of aromatic compounds. *Sens. Actuators B Chem.* **2009**, *139*, 532–537. [[CrossRef](#)]
29. Su, Y.-L.; Li, J.-R.; Jiang, L. A study on the interactions of surfactants with phospholipid/polydiacetylene vesicles in aqueous solutions. *Colloids Surfaces A Physicochem. Eng. Asp.* **2005**, *257–258*, 25–30. [[CrossRef](#)]
30. de Oliveira, C.P.; Soares, N.D.F.F.; Fontes, E.A.F.; de Oliveira, T.V.; Filho, A.M.M. Behaviour of polydiacetylene vesicles under different conditions of temperature, pH and chemical components of milk. *Food Chem.* **2012**, *135*, 1052–1056. [[CrossRef](#)]
31. Kolusheva, S.; Shahal, T.; Jelinek, R. Cation-Selective Color Sensors Composed of Ionophore–Phospholipid–Polydiacetylene Mixed Vesicles. *J. Am. Chem. Soc.* **2000**, *122*, 776–780. [[CrossRef](#)]
32. Friedman, S.; Kolusheva, S.; Volinsky, R.; Zeiri, L.; Schrader, T.; Jelinek, R. Lipid/Polydiacetylene Films for Colorimetric Protein Surface-Charge Analysis. *Anal. Chem.* **2008**, *80*, 7804–7811. [[CrossRef](#)] [[PubMed](#)]
33. Kolusheva, S.; Zadnarm, R.; Schrader, T.; Jelinek, R. Color Fingerprinting of Proteins by Calixarenes Embedded in Lipid/Polydiacetylene Vesicles. *J. Am. Chem. Soc.* **2006**, *128*, 13592–13598. [[CrossRef](#)]
34. Hartmann, H. Ein einfacher weg zu neuartigen borhaltigen spiroverbindungen. *J. Für Prakt. Chemie* **1986**, *328*, 755–762. [[CrossRef](#)]
35. Klein, C.; Baranoff, E.; Nazeeruddin, K.; Grätzel, M. Convenient synthesis of functionalized 4,4'-disubstituted-2,2'-bipyridine with extended π -system for dye-sensitized solar cell applications. *Tetrahedron Lett.* **2010**, *51*, 6161–6165. [[CrossRef](#)]
36. Akhmadeev, B.; Podyachev, S.; Katsyuba, S.; Spicher, S.; Sudakova, S.; Gimazetdinova, G.S.; Syakaev, V.; Sinyashin, O.; Mustafina, A. The incorporation of upper vs lower rim substituted thia- and calix[4]arene ligands into polydiacetylene polymeric bilayers for rational design of sensors to heavy metal ions. *Polymer* **2022**, *245*, 124728. [[CrossRef](#)]

37. Sheldrick, G. *SADABS*; Program for Empirical X-ray Absorption Correction; Bruker-Nonius, University of Gottingen: Gottingen, Germany, 2004.
38. Sheldrick, G. *SHELXTL*, v.6.12; Structure Determination Software Suite: Bruker AXS: Madison, WI, USA, 2000.
39. *APEX3*, Version 2018.7-2; BrukerAXS Inc.: Madison, WI, USA, 2016.
40. Farrugia, L.J. *WinGX* suite for small-molecule single-crystal crystallography. *J. Appl. Crystallogr.* **1999**, *32*, 837–838. [[CrossRef](#)]
41. Bruno, I.J.; Cole, J.C.; Edgington, P.R.; Kessler, M.; Macrae, C.F.; McCabe, P.; Pearson, J.; Taylor, R. New software for searching the Cambridge Structural Database and visualizing crystal structures. *Acta Crystallogr. Sect. B Struct. Sci.* **2002**, *58*, 389–397. [[CrossRef](#)]
42. Pracht, P.; Bohle, F.; Grimme, S. Automated exploration of the low-energy chemical space with fast quantum chemical methods. *Phys. Chem. Chem. Phys.* **2020**, *22*, 7169–7192. [[CrossRef](#)]
43. Grimme, S.; Bohle, F.; Hansen, A.; Pracht, P.; Spicher, S.; Stahn, M. Efficient Quantum Chemical Calculation of Structure Ensembles and Free Energies for Nonrigid Molecules. *J. Phys. Chem. A* **2021**, *125*, 4039–4054. [[CrossRef](#)]
44. Grimme, S.; Hansen, A.; Ehlert, S.; Mewes, J.-M. r²SCAN-3c: A “Swiss army knife” composite electronic-structure method. *J. Chem. Phys.* **2021**, *154*, 064103. [[CrossRef](#)] [[PubMed](#)]
45. Klamt, A.; Diedenhofen, M. Calculation of Solvation Free Energies with DCOSMO-RS. *J. Phys. Chem. A* **2015**, *119*, 5439–5445. [[CrossRef](#)] [[PubMed](#)]
46. Eckert, F.; Klamt, A. Fast solvent screening via quantum chemistry: COSMO-RS approach. *AIChE J.* **2002**, *48*, 369–385. [[CrossRef](#)]
47. Eckert, F.; Klamt, A. *COSMO Therm, Release 19*; COSMOlogic GmbH & Co. KG: Leverkusen, Germany, 2012.
48. Spicher, S.; Grimme, S. Single-point Hessian calculations for improved vibrational frequencies and rigid-rotor-harmonic-oscillator thermodynamics. *J. Chem. Theory Comput.* **2021**, *17*, 1701–1714. [[CrossRef](#)] [[PubMed](#)]
49. Grimme, S. Supramolecular Binding Thermodynamics by Dispersion-Corrected Density Functional Theory. *Chem.—A Eur. J.* **2012**, *18*, 9955–9964. [[CrossRef](#)]
50. Spicher, S.; Grimme, S. Efficient Computation of Free Energy Contributions for Association Reactions of Large Molecules. *J. Phys. Chem. Lett.* **2020**, *11*, 6606–6611. [[CrossRef](#)]
51. Bannwarth, C.; Ehlert, S.; Grimme, S. GFN2-xTB—An Accurate and Broadly Parametrized Self-Consistent Tight-Binding Quantum Chemical Method with Multipole Electrostatics and Density-Dependent Dispersion Contributions. *J. Chem. Theory Comput.* **2019**, *15*, 1652–1671. [[CrossRef](#)]
52. Ehlert, S.; Stahn, M.; Spicher, S.; Grimme, S. Robust and Efficient Implicit Solvation Model for Fast Semiempirical Methods. *J. Chem. Theory Comput.* **2021**, *17*, 4250–4261. [[CrossRef](#)]
53. Gross, E.; Dobson, J.; Petersilka, M.; Nalewajski, R.F. (Eds.) *Density Functional Theory II*; Springer: Berlin/Heidelberg, Germany, 1996; Chapter 181.
54. Casida, M. *Recent Advances in Density Functional Methods*; World Scientific: Hackensack, NJ, USA, 1995.
55. Furche, F. On the density matrix based approach to time-dependent density functional response theory. *J. Chem. Phys.* **2001**, *114*, 5982–5992. [[CrossRef](#)]
56. Adamo, C.; Barone, V. Toward reliable density functional methods without adjustable parameters: The PBE0 model. *J. Chem. Phys.* **1999**, *110*, 6158–6170. [[CrossRef](#)]
57. Eichkorn, K.; Treutler, O.; Öhm, H.; Häser, M.; Ahlrichs, R. Auxiliary basis sets to approximate Coulomb potentials. *Chem. Phys. Lett.* **1995**, *240*, 283–290. [[CrossRef](#)]
58. Eichkorn, K.; Weigend, F.; Treutler, O.; Ahlrichs, R. Auxiliary basis sets for main row atoms and transition metals and their use to approximate Coulomb potentials. *Theor. Chem. Accounts* **1997**, *97*, 119–124. [[CrossRef](#)]
59. Weigend, F.; Häser, M.; Patzelt, H.; Ahlrichs, R. RI-MP2: Optimized auxiliary basis sets and demonstration of efficiency. *Chem. Phys. Lett.* **1998**, *294*, 143–152. [[CrossRef](#)]
60. Spicher, S.; Plett, C.; Pracht, P.; Hansen, A.; Grimme, S. Automated Molecular Cluster Growing for Explicit Solvation by Efficient Force Field and Tight Binding Methods. *J. Chem. Theory Comput.* **2022**, *18*, 3174–3189. [[CrossRef](#)] [[PubMed](#)]
61. Grimme, S.; Bannwarth, C.; Caldeweyher, E.; Pisarek, J.; Hansen, A. A general intermolecular force field based on tight-binding quantum chemical calculations. *J. Chem. Phys.* **2017**, *147*, 161708. [[CrossRef](#)]
62. Spicher, S.; Grimme, S. Robust atomistic modeling of materials, organometallic, and biochemical systems. *Angew. Chem. Int. Ed.* **2020**, *59*, 15665–15673. [[CrossRef](#)]
63. Furche, F.; Ahlrichs, R.; Hättig, C.; Klopper, W.; Sierka, M.; Weigend, F. TURBOMOLE V7.5.1 2021, a Development of University of Karlsruhe and Forschungszentrum Karlsruhe GmbH, 1989–2007, TURBOMOLE GmbH Since 2007. Available online: <http://www.turbomole.com> (accessed on 1 January 2023).
64. Cornago, M.D.P.; Cabildo, P.; Sanz, D.; Claramunt, R.M.; Torralba, M.C.; Torres, M.R.; Elguero, J. Structures of Hemi-Curcuminoids in the Solid State and in Solution. *Eur. J. Org. Chem.* **2013**, *2013*, 6043–6054. [[CrossRef](#)]
65. Tsaplev, Y.B.; Lapina, V.A.; Trofimov, A.V. Fluorescence of curcumin in alkaline dimethyl sulfoxide and the effects of alkali metal cations on it. *J. Photochem. Photobiol. A Chem.* **2021**, *405*, 112967. [[CrossRef](#)]
66. Gobrogge, C.A.; Kong, V.A.; Walker, R.A. Temperature Dependent Solvation and Partitioning of Coumarin 152 in Phospholipid Membranes. *J. Phys. Chem. B* **2015**, *120*, 1805–1812. [[CrossRef](#)]
67. Goto, M.; Wilk, A.; Kazama, A.; Chodankar, S.; Kohlbrecher, J.; Matsuki, H. Chain elongation of diacylphosphatidylcholine induces fully bilayer interdigitation under atmospheric pressure. *Colloids Surfaces B Biointerfaces* **2011**, *84*, 44–48. [[CrossRef](#)]

68. Elistratova, J.; Akhmadeev, B.; Zairov, R.; Dovzhenko, A.; Podyachev, S.; Sudakova, S.; Syakaev, V.; Jelinek, R.; Kolusheva, S.; Mustafina, A. Tb(III) complexes with nonyl-substituted calix[4]arenes as building blocks of hydrophilic luminescent mixed polydiacetylene-based aggregates. *J. Mol. Liq.* **2018**, *268*, 463–470. [[CrossRef](#)]
69. Gerasimova, T.P.; Burganov, T.I.; Katsyuba, S.A.; Kalinin, A.A.; Islamova, L.N.; Fazleeva, G.M.; Ahmadeev, B.S.; Mustafina, A.R.; Monari, A.; Assfeld, X.; et al. Halochromic luminescent quinoxalinones as a basis for pH-sensing in organic and aqueous solutions. *Dye. Pigment.* **2021**, *186*, 108958. [[CrossRef](#)]
70. Tanaka, H.; Gomez, M.A.; Tonelli, A.E.; Lovinger, A.J.; Davis, D.D.; Thakur, M. Structural and morphological study of a melt-crystallized polydiacetylene. *Macromolecules* **1989**, *22*, 2427–2432. [[CrossRef](#)]
71. Jiang, H.; Jelinek, R. Mixed Diacetylene/Octadecyl Melamine Nanowires Formed at the Air/Water Interface Exhibit Unique Structural and Colorimetric Properties. *Langmuir* **2015**, *31*, 5843–5850. [[CrossRef](#)] [[PubMed](#)]
72. Kwon, J.H.; Song, J.E.; Yoon, B.; Kim, J.M.; Cho, E.C. Role of Gel to Fluid Transition Temperatures of Polydiacetylene Vesicles with 10,12-Pentacosadiynoic Acid and Cholesterol in Their Thermochromisms. *Bull. Korean Chem. Soc.* **2014**, *35*, 1809–1816. [[CrossRef](#)]
73. Pan, X.; Wang, Y.; Jiang, H.; Zou, G.; Zhang, Q. Benzo-15-crown-5 functionalized polydiacetylene-based colorimetric self-assembled vesicular receptors for lead ion recognition. *J. Mater. Chem.* **2011**, *21*, 3604–3610. [[CrossRef](#)]
74. Jose, D.A.; König, B. Polydiacetylene vesicles functionalized with N-heterocyclic ligands for metal cation binding. *Org. Biomol. Chem.* **2010**, *8*, 655–662. [[CrossRef](#)] [[PubMed](#)]
75. Wang, M.; Wang, F.; Wang, Y.; Zhang, W.; Chen, X. Polydiacetylene-based sensor for highly sensitive and selective Pb²⁺ detection. *Dye. Pigment.* **2015**, *120*, 307–313. [[CrossRef](#)]
76. Guo, J.; Yang, L.; Zhu, L.; Chen, D. Selective detection of metal ions based on nanocrystalline ionochromic polydiacetylene. *Polymer* **2013**, *54*, 743–749. [[CrossRef](#)]
77. Batys, P.; Morga, M.; Bonarek, P.; Sammakorpi, M. pH-Induced Changes in Polypeptide Conformation: Force-Field Comparison with Experimental Validation. *J. Phys. Chem. B* **2020**, *124*, 2961–2972. [[CrossRef](#)]
78. Jurrus, E.; Engel, D.; Star, K.; Monson, K.; Brandi, J.; Felberg, L.E.; Brookes, D.H.; Wilson, L.; Chen, J.; Liles, K.; et al. Improvements to the APBS biomolecular solvation software suite. *Protein Sci.* **2017**, *27*, 112–128. [[CrossRef](#)] [[PubMed](#)]

Disclaimer/Publisher's Note: The statements, opinions and data contained in all publications are solely those of the individual author(s) and contributor(s) and not of MDPI and/or the editor(s). MDPI and/or the editor(s) disclaim responsibility for any injury to people or property resulting from any ideas, methods, instructions or products referred to in the content.